Computers and Mathematics with Applications 64 (2012) 1065–1083

Contents lists available at SciVerse ScienceDirect

Computers and Mathematics with Applications

journal homepage: www.elsevier.com/locate/camwa

Application of lattice Boltzmann method to the fluid analysis in a rectangular microchannel

Chyung Ay, Chao-Wang Young *, Chuen-Fu Young

Department of Biomechatronic Engineering, National Chiayi University, No.300, Syuefu Rd., East Dist., Chiayi, Taiwan

ARTICLE INFO

Keywords:
Lattice Boltzmann method
Microfluid
Biological particle
Cavity flow
D2Q9

ABSTRACT

The lattice Boltzmann method (LBM) is a computation and modeling method different from traditional numerical methods. It has unique features that other numerical methods do not have due to its micro-particle characterization. The present study includes solving cavity flow problems, writing graphical interface programs for two-dimensional nine-velocity (D2Q9) modeling, and drawing the collision and flow process with Reynolds number 400 and relaxation factor 1.5. The LBM led to the same converged solutions of cavity flow obtained by traditional computational fluid dynamics. In addition, LBM was also used to simulate pipe flow in a rectangular microchannel and investigate the effect of drag force, dielectrophoresis, and buoyancy on the motion of biological particles. The equation of motion for biological particles under drag force, dielectrophoresis, and buoyancy was utilized to simulate the pipe flow and microparticle flow in a microchannel. Spiral flow lines were clearly found near microelectrodes. The calculation was carried out for the pressure drop of fluids at concentrations of 0.13 to 10^{-6} M under 0.25 V AC field. Flow line diagrams were drawn for fluids under pressure gradients. The flow line diagram shows that a spiral pattern remains near the electrodes, whereas flow lines away from the electrodes move towards the right direction, when the pressure gradient is 10^2 and velocity of horizontal and vertical components is 6. This observation means that the biological particles inside the strong electric field are adsorbed on the electrodes, whereas those away from electrodes and inside the weak electric field are flushed out. Thus, this rectangular microchannel is able to separate biological particles. The simulation results from the study hopes to provide further understanding of electroosmotic flow and promote its application development in microelectromechanical systems and biomedical fields.

1. Introduction

In recent years, micro-nanotechnology has received increasing attention from both the industry and the academy. Controlling objects in a micro–nano scale has become a popular subject. Biotechnology R&D is one key point in this development, including quick and accurate identification of pathogenic parasites, bacteria, and virus, as well as determination of adequate drug treatments. A new technology from microelectromechanical systems (MEMSs) and nanotechnology fields utilizes dielectrophoresis to control colloid particles or biological particles, such as blood cells, bacteria, and viruses in a micro or nano scale. Based on the microchannel theory by Henrik in 2005 [1], the present study investigates the effects of AC electroosmosis and electrophoresis on biological particles in a rectangular microchannel under external 0.25 V AC voltage on electrodes.

* Corresponding author. Fax: +886 5 2717647.
E-mail address: youngcw@mail.ncyu.edu.tw (C.-W. Young).

0898-1221/$ – see front matter Crown Copyright © 2012 Published by Elsevier Ltd. All rights reserved.
doi:10.1016/j.camwa.2012.03.025

Nomenclature

a, r	Particle radius
α	Polarizability
d	Insulator thickness
E	Electric field
ε_m	Liquid dielectric constant
ε_p	Particle dielectric constant
F	Faraday constant
f	Body force
g	Gravity
p	Pressure
ϕ, ψ	Electric potential
q^{-1}	Spatial modulation
R	Mole gas constant
T	Absolute temperature
u	Liquid speed
$\vec{u}$	Liquid speed vector
υ	Particle speed
$\vec{\upsilon}$	Particle speed vector
ω	Angular frequency
ζ	Zeta potential

The micro fluidic system study is frequently adopted in biomedical and high-tech industries because various MEMS application systems involve mass transfer, heat transfer, and ion polarization. The medical applications of this system include timely and proper drug delivery, accurate and fast identification of DNA protein organics, and biological particle operation and structure predication [2]. Its high-tech industrial applications include biochip utilizing micro fluidic system for mass or heat transfer, atomic force microscopy, and so on.

Researchers attempted to fabricate a micropump, an alternative to traditional mechanical micropumps, which are uneconomical and difficult to manufacture and maintain, due to MEMS R&D needs. In the natural world, various substances carry very small amounts of charge distribution due to hydrolysis or static electricity. Thus, mechanical micropump alternatives use external electric fields to drive the motion of electric charges in a solution inside a microflow channel. The electro-osmosis effect is utilized to drive a microchannel fluid to achieve mass and heat transfer in the MEMS system [3,4]. After electrophoresis, dielectrophoresis, electroosmosis, streaming potential, and sedimentation potential found applications in fluid mass transfer for colloidal particles and biological particles, similar examples have existed for electrodynamics [5].

The present study models electroosmotic flow in a micro scale and seeks numerical solutions to assist future development in MEMS or mechanics in an even smaller scale. The LBM [6] is adopted as the numerical method. The theory of this method is based on collision behavior among particles and on simulation with equations on a microscopic scale. This theory is different from traditional computational fluid dynamics (CFD), which applies equations of fluid dynamics on a macroscopic scale. Although traditional numerical computation is applicable in macro and micro scales, it does not assure that the system complies to current equations on macro scale. Thus, the present study adopts LBM to assure accuracy and applicability on a microscopic scale. Through particle collision angles, the said method can simulate on a smaller computation range compared with traditional numerical methods for electroosmosis fluids, thus meeting the trend of future industrial technology developments.

2. Experiment equipment and method

The present study uses a PC (Intel® Pentium® 3.00 GHz, 1 G RAM) and Borland C++Builder 6.0 with Matlab 6.5 to write a program in solving cavity flow. The present study also uses the LBM to simulate the flow of fluids in the microchannel [7]. The physics in the microchannel is extremely complicated due to the coexistence of electricity, magnetic, convection, conduct, and radiation. Thus, using a mathematical model to describe the complicated fluid and chemical flow and heat transfer is a challenge. Before the investigation using a mathematical model, several assumptions were set, listed as follows:

(1) The fluid is Newtonian fluid.
(2) Flow field is non-compressible.
(3) Joule heating effect due to external electric field is not considered.
(4) No chemical reaction occurs.

The microchannel system contains a thin glass plate and a flow channel path. An electrolyte solution is placed between the glass plates. Compared with the flow channel, the Debye thickness of the electric double layer is small. Therefore, computation based on traditional macroscopic fluid dynamics is problematic. The theory and concept for microchannels involve the complicated interactions between electromagnetic force and fluids from electro-viscous effect, electroosmotic flow, electrophoresis, colloids, and so on. The electric double layer thickness is only nonsocial, thus, it has very little effect on the microchannel. Further, the LBM can easily handle interaction on micro or molecular scale.

2.1. Dielectrophoresis effect

The dielectrophoresis separation technique induces shift for charged or neutral particles via electric field induction (polarization) under a non-uniform electric field (DC/AC). Adsorption and repulsion among particles manifests a dielectrophoresis force. This phenomenon is determined by the degree of polarization between the particles and the solution. In addition, both the direction and the magnitude of the dielectrophoresis force are related to frequency, particle surface charge, and neighbor free charges.

The principle of the dielectrophoresis force is for charged particles to move towards the electrode in a direction opposite to the charge type. The separation is achieved by applying an electric field in the separation channel and allowing different particles to move in the direction of an electric field according to their charge type and molecular conformation. Any substance due to ionization or surface adsorption of other charged substance will move to the opposite electrode.

Aside from being affected by charges, electrophoresis separation is also affected by electric field strength, solution pH value, solution ionic strength (concentration), electroosmotic flow, and temperature.

The dielectrophoresis effect was proposed by Pohl in 1951 to describe particle movement due to polarization under a non-uniform electric field. When dielectrophoresis force F_{DEP} is applied to a spherical particle, it can be expressed by the following equation:

$$F_{DEP} = \mathrm{Re}\{[m(\omega) \cdot \nabla]E\} \tag{1}$$

where Re{} represents the real part, E is electric field magnitude, and $m(\omega)$ is the induced dipole moment for microsphere under electric field, which is expressed as follows:

$$m(\omega) = 4\pi\varepsilon_m r^3 K(\omega)E \tag{2}$$

$$K(\omega) = \frac{\varepsilon_p^* - \varepsilon_m^*}{\varepsilon_p^* + 2\varepsilon_m^*} \tag{3}$$

where ε_m is the permittivity of suspension solution, r is microsphere radius, ω is the angular frequency for applied electric field, and ε_m^* and ε_p^* are the complex permittivity for solution and microparticle, respectively. In addition, $\varepsilon^* = \varepsilon - j\sigma/\omega$, where ε is dielectric constant and σ is the conductivity. Finally, Eq. (1) can be re-written as:

$$F_{DEP} = 2\pi\varepsilon_m r^3 \mathrm{Re}[K(\omega)]\nabla E^2. \tag{4}$$

The equation shows that the magnitude changes with frequency, and whether the microparticle has larger polarization than the suspension solution. Micro-particles will move in the direction of the high electric field, which is called the positive dielectrophoresis effect when $\mathrm{Re}[K(\omega)]$ is a positive value. In contrast, the microparticles will repulse the high electric field and will move towards the direction of the low electric field, which is called negative dielectrophoresis when $\mathrm{Re}[K(\omega)]$ is a negative value. Thus, an electric field with different strength can be generated by the different design of the electrode compartment or micro-column array in the microchannel. Subsequently, particles can be concentrated or separated (e.g., cells) in the solution by positive or negative dielectrophoresis forces.

Induced dipole moments in a non-uniform electric field generate dielectrophoresis forces, causing the particles to move. The forces that acted on the two ends of the dipole moment are either both the same or both the opposite, no movement is created if the electric field is uniform. The dipole moment of electric charge ($p = Qd$) in a non-uniform electric field will generate different Coulomb forces when subjected to different electric fields. The force is therefore related to the product of the dipole moment and the external electric field. Fig. 1 shows different forces generated for two charges of a dipole moment in $p = Qd$ in a non-uniform electric field E, i.e.,

$$F = QE(r + d) - QE(r). \tag{5}$$

Fig. 1 shows that the negative charge is located in the vector r value. If d length is very small, electric field $E(r)$ can be expanded by Taylor series and the force is given by

$$F = QE(r) + Q\left(d_x\frac{\partial}{\partial x} + d_y\frac{\partial}{\partial y} + d_z\frac{\partial}{\partial z}\right)E(r) - QE(r). \tag{6}$$

After omitting the first and the last terms and the high-order terms, the above equation for dielectrophoresis force is given by

$$F_{DEP} = (p \cdot \nabla)E. \tag{7}$$

From the equation, the dielectrophoresis force in a uniform electric field is zero, i.e. dielectrophoresis force is only generated in a non-uniform electric field.

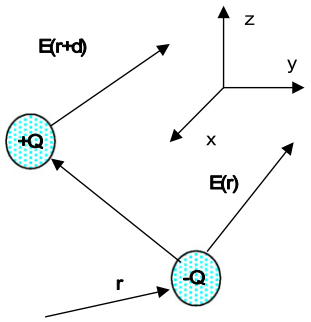

Fig. 1. Charge dipole moment.

2.2. Drag force

The effects of drag force [8], dielectrophoresis, and buoyancy on biological particle movement in a rectangular microchannel was studied based on the investigation by Thomas et al. [8] after obtaining steady-state velocity for a fluid using the lattice Boltzmann method. The equation of motion for the biological particle subject to drag force, dielectrophoresis, and buoyancy was then derived.

Assuming a spherical particle of radius a and velocity υ in a liquid and u as fluid velocity without particles, the drag force (Stokes drag force) due to particle friction can be expressed by:

$$F_{st} = 6\pi\eta a(u - \upsilon). \tag{8}$$

If the particle in the water is stagnant, it usually takes approximately 5 μs to reach the steady-state velocity. This is the reason why acceleration was not considered.

2.3. Lattice Boltzmann method

Fluids (e.g. air and water) are the most common substances in the natural world. The interaction among fluid molecules is small, thus, deformation can still occur even under a very small external force. In most situations, it is plausible to assume that fluids are in a continuum. Under this assumption, although clear differences may exist among different fluids (e.g., gas and liquid), they all follow the same principle of motion. In mathematics, the macroscopic motion for fluids can be described by nonlinear partial differential equation, i.e., the Navier–Stokes equation.

Numerical simulation has become an important means and tool for fluid dynamics due to the advancement of computer technology. Consequently, it has received increasing attention. The numerical simulation field has developed a new discipline called computational fluid dynamics (CFD). The design of the numerical method to simulate fluid motion includes two approaches: top-down based on a macroscopic continuous model and bottom-up based on a microscopic discrete model. Numerical methods in traditional fluid dynamics are mostly designed by top-down approach. Moreover, a microscopic model that can keep real fluid characteristics in a simple structure was built to describe particle motion as simple as possible and allow the macroscopic characteristics to comply to subjective motion principles. Thus, a real fluid system was simulated using an artificial model on a microscopic scale.

In recent years, the LBM that received significant attention is different from the traditional numerical method for fluid computation and modeling. At present, aside from successful application in fluid dynamics, LBM can also be successfully applied in multiphase flow, seepage flow, and magnetic fluid dynamics, among others. LBM is in a stage of continuous development. Its basic theory, model, and applications have significantly advanced in recent years.

3. Numerical simulation method

To apply Newton's second law to a microfluidic system, the acceleration vector field $\vec{a}$ in flow field first needs to be figured out. Thus, the full-time derivative, which is also called a substantial derivative or a material derivative for the velocity vector, will be calculated. The concept can be applied to any variable.

$$\vec{a} = \frac{d\vec{N}}{dt} = \vec{i}\frac{du_x}{dt} + \vec{j}\frac{du_y}{dt} + \vec{k}\frac{du_z}{dt}. \tag{9}$$

Each scalar component (u_x, u_y, u_z) is a variable for four variables (x, y, z, t), thus, the chain rule is used to obtain the time derivative for each scalar. For example,

$$\frac{du_x(x, y, z, t)}{dt} = \frac{\partial u}{\partial t} + \frac{\partial u}{\partial x}\frac{dx}{dt} + \frac{\partial u}{\partial y}\frac{dy}{dt} + \frac{\partial u}{\partial z}\frac{dz}{dt}. \tag{10}$$

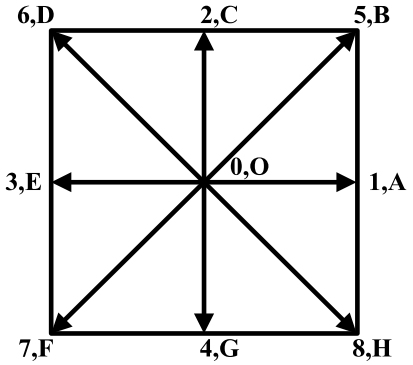

Fig. 2. D2Q9 model structure and velocity component diagram.

Based on the definition, dx/dt represents the local velocity component v_x, whereas $\frac{dy}{dt} = v_y$ and $\frac{dz}{dt} = v_z$, the full derivative for $\vec{u}$ can be further expressed as the following simple form:

$$\vec{a} = \frac{\partial \vec{u}}{\partial t} + v_x \frac{\partial \vec{u}}{\partial x} + v_y \frac{\partial \vec{u}}{\partial y} + v_z \frac{\partial \vec{u}}{\partial z} = \frac{\partial \vec{u}}{\partial t} + (\vec{v} \cdot \nabla)\,\vec{u} \tag{11}$$

where $\frac{\partial \vec{u}}{\partial t}$ term is called local acceleration, which is zero in steady-state flow, i.e., independent from time. $(\vec{v} \cdot \nabla)\,\vec{u}$ is called convective acceleration, which is generated as a fluid particle passes through an area with spatial velocity change, such as a nozzle or diffuser. Further, a very large acceleration may be generated due to convection even for a stable flow field in a normal state.

In the above Eq. (11), a concise inner product form was used, which involves velocity $\vec{v}$ and gradient operator, ∇:

$$v_x \frac{\partial}{\partial x} + v_y \frac{\partial}{\partial y} + v_z \frac{\partial}{\partial z} = (\vec{v} \cdot \nabla) \quad \text{in which } \nabla = \vec{i}\frac{\partial}{\partial x} + \vec{j}\frac{\partial}{\partial y} + \vec{k}\frac{\partial}{\partial z}.$$

3.1. Lattice Boltzmann method BGK collision approximate equation

LBM starts with Boltzmann equation:

$$\frac{Df}{Dt} = \frac{\partial f}{\partial t} + \nu \nabla f = Q. \tag{12}$$

The equation describes the change of distribution function for particles through collision and transfer. f is the density distribution function, ν is the velocity, and Q is the collision operator. The assumption is that the collision takes place between two particles only, that no external force is involved in the collision process, and that particle velocity after collision is unaffected by the velocity before collision. The collision operator drives the distribution function towards Maxwell distribution. Eq. (12) after time and spatial discrete is given by the following equation:

$$\frac{f(x, t+\delta_t) - f(x, t)}{\delta_t} + \frac{f(x + v\delta_t, t+\delta_t) - f(x, t+\delta_t)}{\delta_t} = Q \tag{13}$$

(i.e. $\frac{Df}{Dt} = \lim_{\delta_t \to 0} \frac{f(x+v\delta_t, t+\delta_t) - f(x,t)}{\delta_t} = Q$) which can be further simplified as:

$$f(x + v\delta_t, t + \delta_t) - f(x, t) = Q\delta_t. \tag{14}$$

The study adopts the D2Q9 model for the particle lattice. The lattice model is as in Fig. 2, in which $\alpha = 0, 1, \ldots, 8$ represents each lattice element and e_α represent each element velocity, with definition as follows:

$$\left.\begin{array}{l} e_0 = (0, 0), \\ e_1 = \overrightarrow{OA} = (c, 0), e_2 = \overrightarrow{OC} = (0, c), e_3 = \overrightarrow{OE} = (-c, 0), e_4 = \overrightarrow{OG} = (0, -c) \\ e_5 = \overrightarrow{OB} = (c, c), e_6 = \overrightarrow{OD} = (-c, c), e_7 = \overrightarrow{OF} = (-c, -c), e_8 = \overrightarrow{OH} = (c, -c) \end{array}\right\}. \tag{15}$$

In this equation, $c = \frac{\delta_t}{\delta_x} = \sqrt{3RT}$ is the sound velocity, T is the absolute temperature (K), and R is the ideal gas constant.

After lattice transformation, Eq. (14) becomes:

$$f_\alpha(x + e_\alpha\delta_t, t + \delta_t) - f_\alpha(x, t) = \delta_t Q_\alpha, \quad \alpha = 0, 1, \ldots, 8. \tag{16}$$

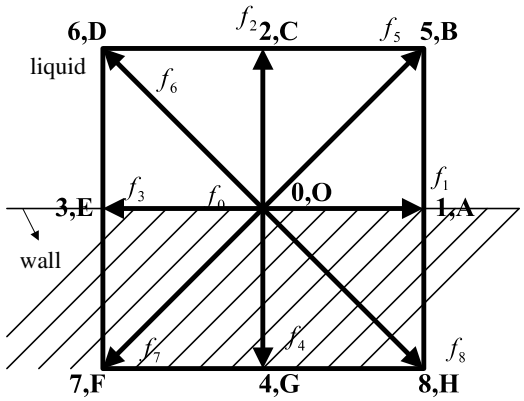

Fig. 3. Bounce back diagram.

For common collision operator Q_α, based on the single particle collision and conservation law, some scholars set the assumption that the collision process approaches Maxwell distribution and proposed that the Boltzmann equation can be approximated to Boltzmann BGK collision approximate equation [9] as follows:

$$f_\alpha(x + e_\alpha\delta_t, t + \delta_t) - f_\alpha(x, t) = -w[f_\alpha(x, t) - f_\alpha^{eq}(x, t)], \quad \alpha = 0, 1, \ldots, 8 \tag{17}$$

where $w = \frac{1}{\tau_v}$ is the relaxation coefficient, τ_v is the relaxation time, δ_t is the step time, δ_x is the step length, and f_α^{eq} is distribution function in equilibrium state.

The Boltzmann method uses Eq. (17) as the basis for numerical computation. Simple derivation was carried out for the distribution function in equilibrium state required by evolution equation in the D2Q9 model and the extrapolation in equilibrium state used in boundary treatment.

Collision step:

$$f_\alpha^{out}(x, t) = (1 - w)f_\alpha(x, t) + wf_\alpha^{eq}(x, t). \tag{18}$$

Streaming step:

$$f_\alpha^{in}(x + e_\alpha\delta_t, t + \delta_t) = f_\alpha^{out}(x, t). \tag{19}$$

Combining collision and streaming equations can obtain the Boltzmann BGK collision approximate equation.

Distribution in equilibrium state can be expressed as follows:

$$f_\alpha^{eq}(x, t) = E_\alpha(\rho, u) = \omega_\alpha\rho\left[1 + \frac{3e_\alpha \cdot u}{c^2} + \frac{9(e_\alpha \cdot u)^2}{2c^4} - \frac{|u|^2}{2c^2}\right] \tag{20}$$

e_α, according to Eq. (15) definition, assumes that $\omega_0 = T_0$, $\omega_1 = \omega_2 = \omega_3 = \omega_4 = T_1$, $\omega_5 = \omega_6 = \omega_7 = \omega_8 = T_2$. Then, the following can be obtained: $c_s = \frac{c}{\sqrt{3}}$, $T_1 = 1/9$, $T_2 = 1/36$, $T_0 = 4/9$, $p = c_s^2\rho$. c_s is called sound velocity.

3.2. Set boundary condition

Usually, fixed-value boundary bounce back treatment is given: the incoming distribution function from collision in a previous time point is equal to the outgoing distribution function after lattice collision in the next time point. For example, when a lattice at the bottom wall boundary is considered, as shown in Fig. 3, it will satisfy the following equation:

$$\left.\begin{array}{l} f_2^{out} = f_4^{in} \\ f_5^{out} = f_7^{in} \\ f_6^{out} = f_8^{in} \end{array}\right\} \tag{21}$$

where f_a^{in}, $a = 4, 7, 8$ is the incoming distribution function, and f_b^{out}, $b = 2, 5, 6$ is the outgoing distribution function at the next time. The main boundary conditions for fluid motion include the following three types: (1) pressure boundary, (2) velocity boundary, and (3) wall boundary.

3.2.1. Pressure boundary

Considering an inlet lattice, as shown in Fig. 3, the pressure is known and Eqs. (22)–(24) can be used to calculate the inlet density. Incoming distribution functions, f_2, f_4, f_0, f_3, f_6, and f_7, are also known. Using $\sum_\alpha f_\alpha = \rho$ and $\sum_\alpha e_\alpha f_\alpha = \rho u$ and the

definition in equilibrium state, the following equations can be derived:

$$f_0 + f_1 + f_2 + f_3 + f_4 + f_5 + f_6 + f_7 + f_8 = \rho_{in} \tag{22}$$
$$f_1 - f_3 + f_5 - f_6 - f_7 + f_8 = \rho_{in} u_1 \tag{23}$$
$$f_2 - f_4 + f_5 + f_6 - f_7 - f_8 = \rho_{in} u_2. \tag{24}$$

Assuming planar coordinates $u = (u_1, u_2)$, the solution is derived as follows:

$$u_1 = 1 - \frac{[f_2 + f_4 + f_0 + 2(f_3 + f_6 + f_7)]}{\rho_{in}}$$
$$f_1 = f_3 + \frac{2}{3}\rho_{in} u_1$$
$$f_5 = f_7 + \frac{1}{2}(f_2 - f_4) + \frac{1}{6}\rho_{in} u_1$$
$$f_8 = f_6 + \frac{1}{2}(f_2 - f_4) + \frac{1}{6}\rho_{in} u_1.$$

These equations can be applied to the inlet pressure boundary condition.

3.2.2. Velocity boundary

Considering an inlet lattice, as shown in Fig. 3, the inlet velocity is known and the incoming distribution functions, f_2, f_4, f_0, f_3, f_6, and f_7, are known. Using $\sum_\alpha f_\alpha = \rho$ and $\sum_\alpha e_\alpha f_\alpha = \rho u$ and the definition in equilibrium state, the following equation can be derived:

$$\rho_{in} = \frac{[f_2 + f_4 + f_0 + 2(f_3 + f_6 + f_7)]}{1 - u_1}$$
$$f_1 = f_3 + \frac{2}{3}\rho_{in} u_1$$
$$f_5 = f_7 + \frac{1}{2}(f_2 - f_4) + \frac{1}{6}\rho_{in} u_1$$
$$f_8 = f_6 + \frac{1}{2}(f_2 - f_4) + \frac{1}{6}\rho_{in} u_1.$$

These equations can be applied to the inlet velocity boundary condition.

3.2.3. Wall boundary

Considering the bottom wall boundary, as shown in Fig. 3, the velocity is known, and the incoming distribution functions, f_3, f_9, f_0, f_4, f_7, and f_8, are also known. Using $\sum_\alpha f_\alpha = \rho$ and $\sum_\alpha e_\alpha f_\alpha = \rho u$ and the definition in equilibrium state, the following equation can be derived:

$$\rho_{in} = \frac{[f_1 + f_3 + f_9 + 2(f_4 + f_7 + f_8)]}{1 - u_2}$$
$$f_2 = f_4 + \frac{2}{3}\rho_{in} u_2$$
$$f_5 = f_7 - \frac{1}{2}(f_1 - f_3) + \frac{1}{2}\rho_{in} u_1 + \frac{1}{6}\rho_{in} u_2$$
$$f_8 = f_6 + \frac{1}{2}(f_1 - f_3) + \frac{1}{2}\rho_{in} u_1 + \frac{1}{6}\rho_{in} u_2.$$

These equations can be applied to the bottom wall boundary condition.

3.3. AC electric field

As shown in Fig. 4, in which a three-dimensional rectangular microchannel electrodes are under AC voltage. At first, LBM was used to obtain fluid velocity at a steady state. Assuming the external force applied to flow channel $\vec{F} = \rho \vec{G i_x}$ only has an x-direction component, then its y-direction velocity component for the generated Poiseuille flow is 0. Consider from the bottom flow channel wall lattice $j = 0$ to the top flow channel wall lattice $j = n$, and assume flow channel velocity x component is u_j, lattice dividing is as shown in Fig. 5. Node $j = 0$ and $j = n$ are the lower and upper boundaries, respectively.

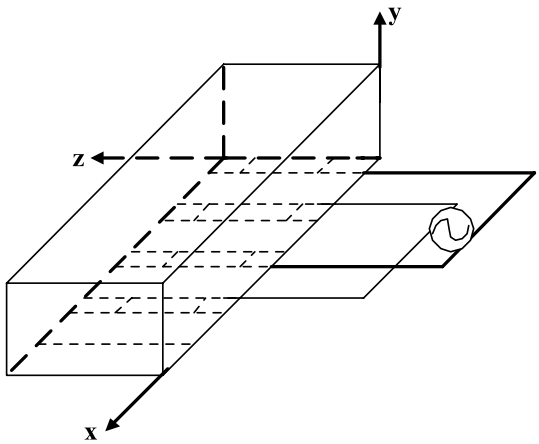

Fig. 4. Three-dimensional diagram for rectangular microchannel.

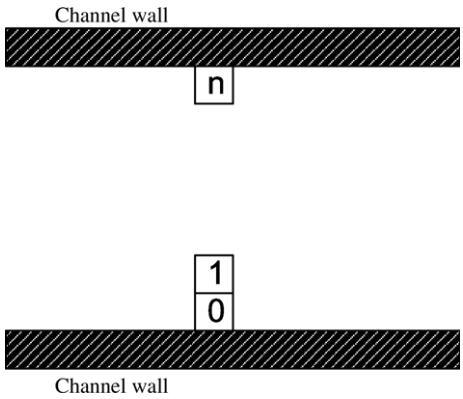

Fig. 5. y-direction lattice division diagram.

Considering the flow field only within lattice $2 \le j \le n-2$, the momentum density ρu_j can be expressed as:

$$\begin{aligned}\rho u_j &= c[(f_1^j - f_3^j) + (f_5^j - f_6^j) + (f_8^j - f_7^j)] = c(1-w)[(f_1^j - f_3^j) + (f_5^{j-1} - f_6^{j-1}) + (f_8^{j+1} - f_7^{j+1})] \\ &\quad + cw\left[(f_1^{eq}(\rho, u_j) - f_3^{eq}(\rho, u_j)) + (f_5^{eq}(\rho, u_{j-1}) - f_6^{eq}(\rho, u_{j-1})) + (f_8^{eq}(\rho, u_{j+1}) - f_7^{eq}(\rho, u_{j+1}))\right] \\ &\quad + \frac{\delta_t^2}{\delta_x}[(g_1 - g_3) + (g_5 - g_6) + (g_8 - g_7)] \\ &= \left[\frac{2}{3}\rho\Phi - \left(1 - \frac{2}{3}\Phi\right)\rho(1-w) + \rho(1-w)w(1-\Phi)\right]u_j \\ &\quad + \left[\frac{1}{6}\rho w\Phi + \left(1 - \frac{2}{3}\Phi\right)\rho(1-w)\right](u_{j-1} + u_{j+1}) + \frac{1}{2c}\rho w\Phi(u_{j-1}v_{j-1} - u_{j+1}v_{j+1}) + \rho\delta_t w\Phi G \end{aligned} \tag{25}$$

in which $\Phi = \exp(-U(x)/k_BT)$ is a factor, a non-uniform characteristic for a single particle. $\tau_v = \frac{1}{w} = \frac{\delta_x}{\delta_t}$, and the external force $F = \rho G i_x$ onto the flow channel only has an x component, thus, the y-direction velocity component in the flow layer of the generated Poiseuille flow is 0. However, the above equation can be simplified as:

$$\left[\left(\frac{4}{3}\Phi - 2\right) + \left(2 - \frac{5}{3}\Phi\right)w + (\Phi - 1)w^2\right]u_j + \left[\left(1 - \frac{2}{3}\Phi\right) + \left(\frac{5}{6}\Phi - 1\right)w\right](u_{j-1} + u_{j+1}) + \frac{\delta_x\Phi wG}{c} = 0. \tag{26}$$

Li and Kwok [10], defined the three parameters ϕ_1, ϕ_2, ϕ_3 [9] as follows:

$$\left.\begin{aligned}\phi_1 &= \left(\frac{4}{3}\Phi - 2\right) w^{-1} + \left(2 - \frac{5}{3}\Phi\right) + (\Phi - 1)w \\ \phi_2 &= \left(1 - \frac{2}{3}\Phi\right) w^{-1} + \left(\frac{5}{6}\Phi - 1\right) \\ \phi_3 &= \frac{\delta_x \Phi G}{c}\end{aligned}\right\}. \tag{27}$$

Eq. (26) can be expressed as:

$$\phi_1 u_j + \phi_2(u_{j-1} + u_{j+1}) + \phi_3 = 0. \tag{28}$$

The solution to Eq. (28) is given by:

$$u_j = -\frac{\phi_3 j(n-j)}{(\phi_1 + 2\phi_2)j(n-j) - 2\phi_2} + U_s. \tag{29}$$

If U_s is the drift velocity per wall condition, the upper boundary $j = n - 1$ is treated as the lower boundary $j = 1$ in Eq. (17) to find the drift velocity. Collision and force at the boundary point is assumed with further bounce back rule. Unknown distribution is predicted as following along the opposite direction:

$$f_2^0 = f_4^0, \qquad f_5^0 = f_7^0 \quad \text{and} \quad f_6^0 = f_8^0.$$

The following equation can be obtained using the corrected bounce back rule:

$$U_s = \phi_3 \left(\frac{\phi_1(n-1)}{(\phi_1 + 2\phi_2)(n-1) - 2\phi_2} + \frac{\phi_1(n-2)}{(\phi_1 + 2\phi_2)(n-2) - \phi_2} - 1 - \frac{2}{3}\tau(\tau - 1) \right) \Big/ (\phi_1 + \phi_2). \tag{30}$$

3.3.1. Equation of motion

The biological particles in a microchannel are subject to the following three types of forces: dielectrophoresis force F_{DEP}, buoyancy F_{gb}, and Stoke drag force F_{st}. Based on Newton's law of motion, the equation of motion for a microparticle can be expressed as follows:

$$m\frac{\partial \upsilon}{\partial t} = F_{st} + F_{DEP} + F_{gb} = 6\pi\eta a(u - \upsilon) + F_{DEP} + (m_f - m_p)g\vec{i}_y \tag{31}$$

where m_p is the particle mass, and m_f is the fluid mass. Through the relationship among density, volume, and mass, $m = 4/3\pi\rho a^3$, the following equation can be obtained after rearrangement:

$$\frac{2\rho_p a^2}{9\eta}\frac{\partial \upsilon}{\partial t} + \upsilon = u + \frac{F_{DEP}}{6\pi\eta a} + \frac{2a^2}{9\eta}(\rho_f - \rho_p)g\vec{i}_y. \tag{32}$$

For a particle 1 μm in water in the system with typical spatial modulation, Stokes value is $St \approx 10^{-5}$. The acceleration term in Eq. (32) can be ignored and leave the steady-state equation of motion as follows:

$$\upsilon = u + \frac{F_{DEP}}{6\pi\eta a} + \frac{2a^2}{9\eta}(\rho_f - \rho_p)g\vec{i}_y. \tag{33}$$

3.4. Cavity flow

LBM can simulate the incompressible Navier–Stokes equation very well when both the grid step length and the Mach number approach zero. The standard D2Q9 and various derivative models are usually used in dealing with two-dimensional problems. All such models use the D2Q9 square lattice. The present study uses cavity flow to seek solutions and adopts the D2Q9 model to validate the accuracy and effectiveness of LBM. The rectangular cavity flow has a variety of geometric structure forms, such as general horizontal rectangular cavity and inclined rectangular cavity. In the current study, the flow field of rectangular cavity was considered to be composed of a horizontal two-dimensional square cavity. The upper boundary of the cavity is a constant velocity for horizontal movement, whereas the other three boundaries remain stagnant, as shown in Fig. 6. The basic characteristic for such a flat plate driving cavity flow is that a primary large swirl exists in the center of the cavity and two secondary swirls at the bottom two corners. The values for the flow field function and the center of swirl are function of the Reynolds number, which is defined as follows:

$$\mathrm{Re} = \frac{LU}{\upsilon} \tag{34}$$

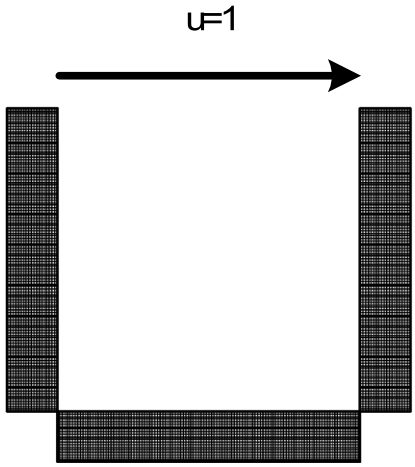

Fig. 6. Rectangular cavity flow.

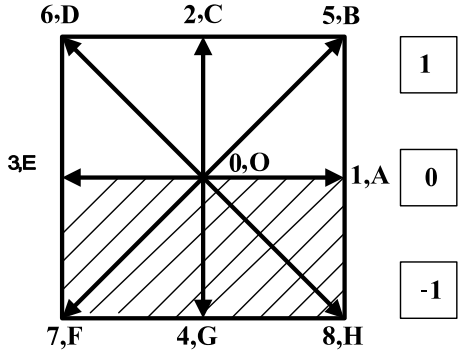

Fig. 7. Boundary diagram.

where L is the cavity height (width), U is the dragging velocity for top plate, and v is the motion viscous coefficient. Simulation is conducted for cavity flow problems with different Reynolds numbers and corresponding relaxation coefficient, ω. The lattice model in use (column/row number 0–260, 261 lattices per column/row) has a fixed size of 261×261.

Researchers have proposed many methods with respect to treating the boundary issue in LBM. However, each of these methods has deficiencies. For example, Zou proposed non-equilibrium bounce-back. Inspired by Zou's non-equilibrium bounce-back [11], Guo et al. [12] proposed a new method to treat the boundary issue, i.e., non-equilibrium extrapolation [12]. The distribution function obtained using this method is more stable than that by linear extrapolation. Non-equilibrium extrapolation also has advantages in wide application scope, simple computation, and easy realization.

The D2Q9 model is used to explain the basic principle for non-equilibrium extrapolation, as shown in Fig. 7. Assuming EOA is located on the boundary, BCD is located in the flow field, FGH is located outside the flow field, and the current system time is t, then the distribution function at the fluid lattice point C is known. To confirm the distribution function at boundary point O, the distribution function $f_\alpha(O, t)$ breaks into two components:

$$f_\alpha(O, t) = f_\alpha^{(eq)}(O, t) + f_\alpha^{(neq)}(O, t) \tag{35}$$

where $f_\alpha^{(neq)}(O, t)$ is the non-equilibrium component.

Velocity boundary condition is used to confirm equilibrium component. Velocity boundary condition $u(O, t)$ is known, whereas density ρ is unknown. Thus, the following virtual equilibrium distribution function can be used to approximate the original equilibrium component:

$$\bar{f}_\alpha^{(eq)}(O, t) = E_\alpha(\rho(C, t), u(O, t)). \tag{36}$$

Non-equilibrium extrapolation equation is given by

$$f_\alpha(O, t) = \bar{f}_\alpha^{(eq)}(O, t) + [f_\alpha(C, t) - f_\alpha^{(eq)}(C, t)]. \tag{37}$$

Generally, the D2Q9 model lattice selection is as shown in Fig. 8. Thus, $M = N = 260$ is selected.

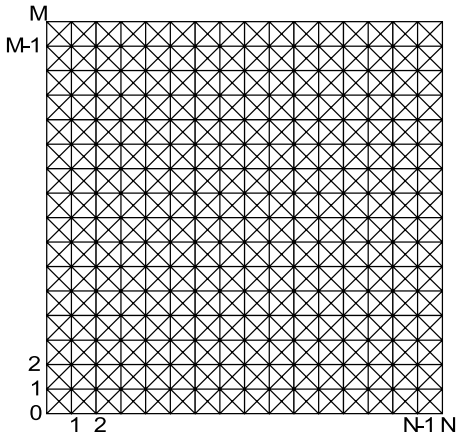

Fig. 8. Cavity flow lattice division diagram.

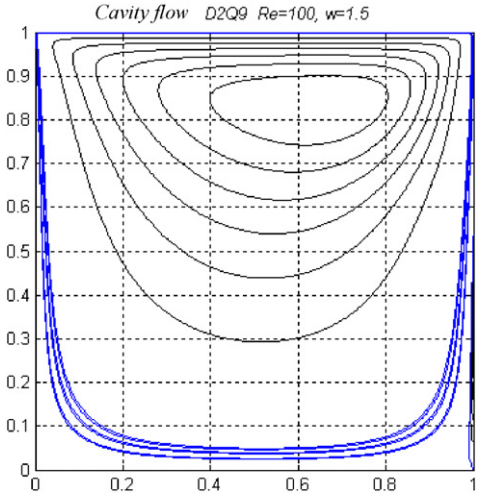

Fig. 9. Flow line diagram, Re = 100 for cavity flow.

4. Results and discussion

LBM based on particle collision behavior can analyze fluid behavior in smaller flow channels. The D2Q9 model can be used to verify the accuracy and effectiveness by finding the cavity flow solution. Therefore, LBM can be used to study the operation of electroosmosis and electrophoresis to drive microparticles to pass a microchannel.

4.1. Cavity flow simulation and discussion

With reference to literature regarding LBM [13,14], and considering the constant velocity horizontal movement as the upper boundary and the stationary state as three other boundaries, the result is drawn as in Fig. 9. The blue line represents the high-speed area and the black lines are equal gradients for the highest flow velocity. Results from the present study match the results from previous studies (Fig. 10) very well. The flow line diagram is plotted with selected recursive frequency, relaxation coefficient, and Reynolds number, as shown in Figs. 11a–11d.

The comparison of Figs. 11a and 11b show that more execution results in lower swirl. The comparison of Figs. 11b and 11c show that higher Reynolds number results in more right swirl. Moreover, the comparison of Figs. 11c and 11d shows that smaller relaxation coefficient (longer relaxation time) results in lower swirl range. The Reynolds number indicates the ratio of inertia force to viscous force acting on a fluid. If change is made to the flow field, the flow line, and velocity distribution: the smaller the Reynolds number, the larger the viscous force, i.e., driving the fluid to the center of channel, the central fluid will be driven by the higher velocity fluid near wall due to viscous force. On the other hand, the larger Reynolds number, the central fluid is dragged less, and the velocity is smaller.

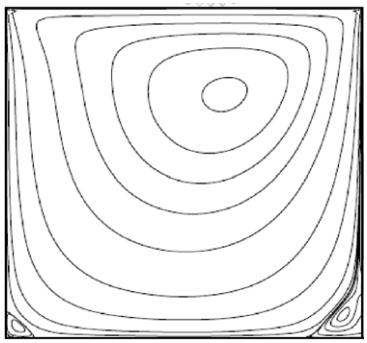

Fig. 10. Flow line diagram, Re = 100 for cavity flow [12,13].

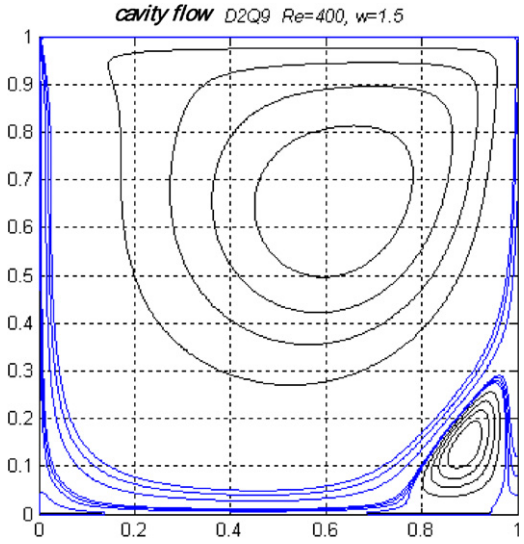

Fig. 11a. Flow line diagram, Re = 400, $w = 1.5$, 22,200 times for cavity flow.

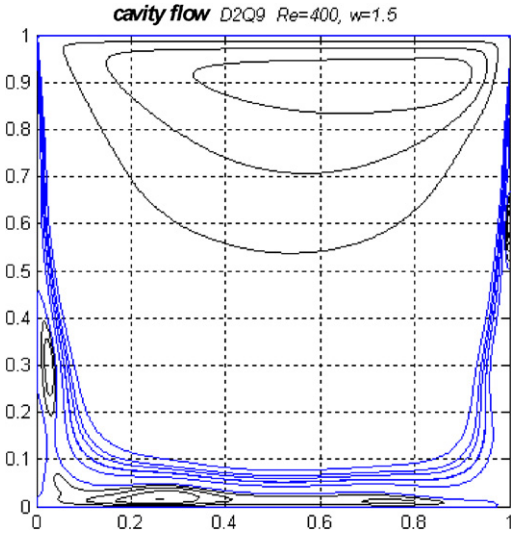

Fig. 11b. Flow line diagram, Re = 400, $w = 1.5$, 2000 times for cavity flow.

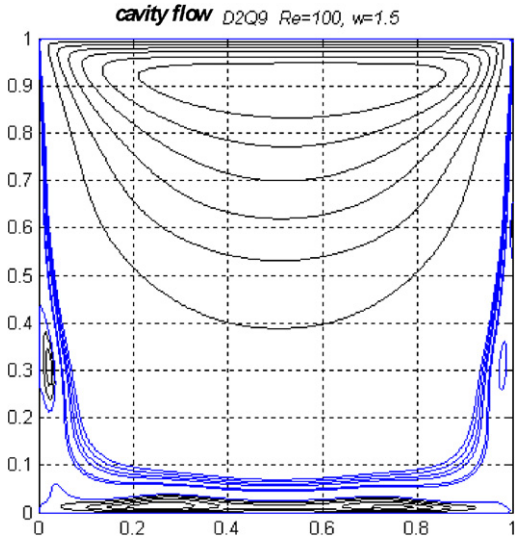

Fig. 11c. Flow line diagram, Re $= 100$, $w = 1.5$, 2000 times for cavity flow.

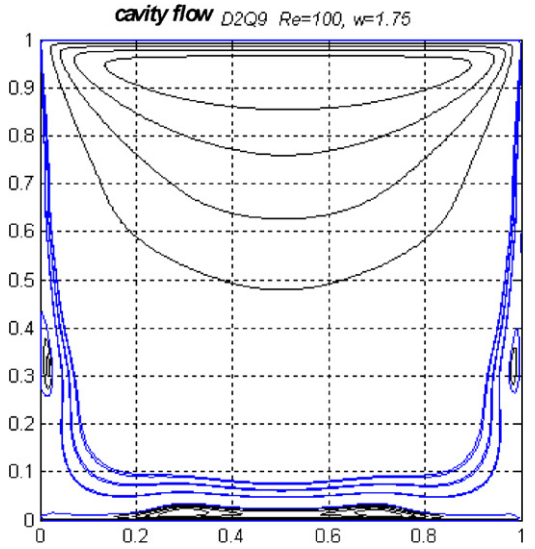

Fig. 11d. Flow line diagram, Re $= 100$, $w = 1.75$, 2000 times for cavity flow.

4.2. Biological particle operation simulation and discussion

Considering n-DEP, assuming particle radius $a = 1.2\,\mu$m, the steady-state equation of motion Eq. (49) for a microparticle in a microchannel, and the influence of pressure drop, $u = u+(u_j, 0)$, u_j is the x component for j lattice by LBM. The equations by Thomas (2006) [8] were modified as follows:

$$\begin{aligned} UXX &= v.*(2.*q.*Y-1).*\exp(-2.*q.*Y).*(\cos(q.*X).*\sin(3.*q.*X) \\ &\quad -\sin(q.*X).*\cos(3.*q.*X)); \\ vuj &= -vphi3.*Y./meshspace.*(vnn\text{-}Y./meshspace)./(vphi4. \\ &\quad *meshspace.*(vnn\text{-}Y./meshspace)-2.*vphi2)+Us; \\ UX &= UXX+vuj. \end{aligned}$$

The time-average velocity UXX generated by electroosmotic flow under AC electric field and the electroosmotic flow velocity vuj due to pressure drop are added together to become the total electroosmotic flow velocity UX. A particle is in a microchannel, as shown in Fig. 4, thus, total field velocity is as shown in Fig. 12. Fig. 12 shows the n-type dielectrophoresis n-DEP, in which all particles in the microchannel are trapped in the inward spiral by the electrode. Numerical analysis is conducted on the operation parameters for biological particles in Table 1. The voltage applied to the electrode is $V \approx$

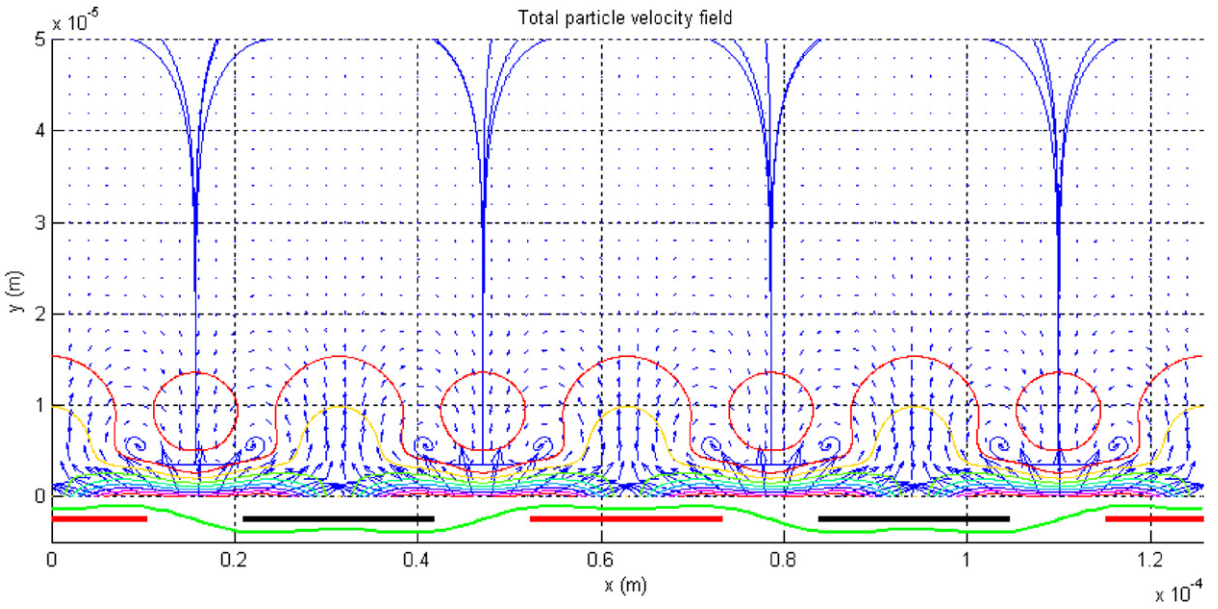

Fig. 12. Total velocity field diagram; particle radius = 1.2 μm.

Table 1
Operation parameter for biological particles.

Parameter	Value	Unit	Description
η	10^{-3}	Pa s	Dynamic viscosity
K	−0.026		CM factor
Λ_D	5.8×10^{-6}	m	Effective length scale
λ_D	8.3×10^{-10}	M	Debye length
q	10^5	m^{-1}	Inverse of spatial modulation
ρ_p	1.05×10^3	$kg\,m^{-3}$	Particle density
σ_p	1.2	$S\,m^{-1}$	Particle conductivity
σ_m	1.3	$S\,m^{-1}$	Liquid conductivity
u_1	2.1×10^{-6}	$m\,s^{-1}$	Maximum velocity for electroosmotic flow
V_0	0.25	V	Electrode potential magnitude
ω_D	1.4×10^9	$rad\,s^{-1}$	Debye frequency
ω^*	5.3×10^6	$rad\,s^{-1}$	Resonance frequency

Table 2
Electrode voltage frequency ω and concentration.

c_0	0.13	10^{-1}	10^{-2}	10^{-3}	10^{-4}	10^{-5}	10^{-6}
ω (rad/s)	5,320,600	4,115,200	450,910	57,547	9694	2215	615
$f = \frac{\omega}{2\pi}$ (Hz)	846,801	654,955	71,765	9159	1543	353	98

$\frac{1}{\pi}(\cos(qx) - \frac{1}{3}\cos(3qx))\exp(i\omega t)V$, frequency ω is according to the equation $\omega = \sqrt{3}q(1+\delta)\lambda_D\omega_D$ [15] proposed by Ajdari in 2000. Based on Table 2, when the concentration is 10^{-4}, the frequency is 9694 rad/s.

In the simulation of biological particle operations, assume that concentration c_0 is 0.13, diffusion constant D is 10^{-9}, insulator thickness d is 10^{-9} m, and capacitance ratio δ is 25. Pressure drop is selected as $dP/dx = 0.1$, 1, 10, and 10^2. Fluid velocity with external pressure drop is calculated and plotted in Figs. 13a–13d.

Figs. 13a–13d indicates that the larger the pressure gradient, the higher the fluid velocity. When $dP/dx = 0.1$, fluid flow is not affected and biological particles remain absorbed onto the electrode, whereas non-absorbed biological particles remain suspended in liquid. When dP/dx is 1, non-absorbed biological particles are flushed away and some are near the electrode, forming double spirals. However, such results are not liked. Non-absorbed biological particles are flushed away and biological particles absorbed on electrode remain when dP/dx is 10, whereas all biological particles are flushed away when dP/dx is 100.

Excluding the limitation by the Joule thermal effect, selecting concentration as 10^{-4}, and setting pressure gradients as $dP/dx = 0.1$, 1, 10, 10^2, 10^3, and 10^4, the total field velocity is drawn as in Figs. 14a–14f. Non-absorbed biological particles are flushed away and some biological particles remain absorbed on the electrode when dP/dx is 10^2. Under this situation, $P_0 = 0.013$ Pa.

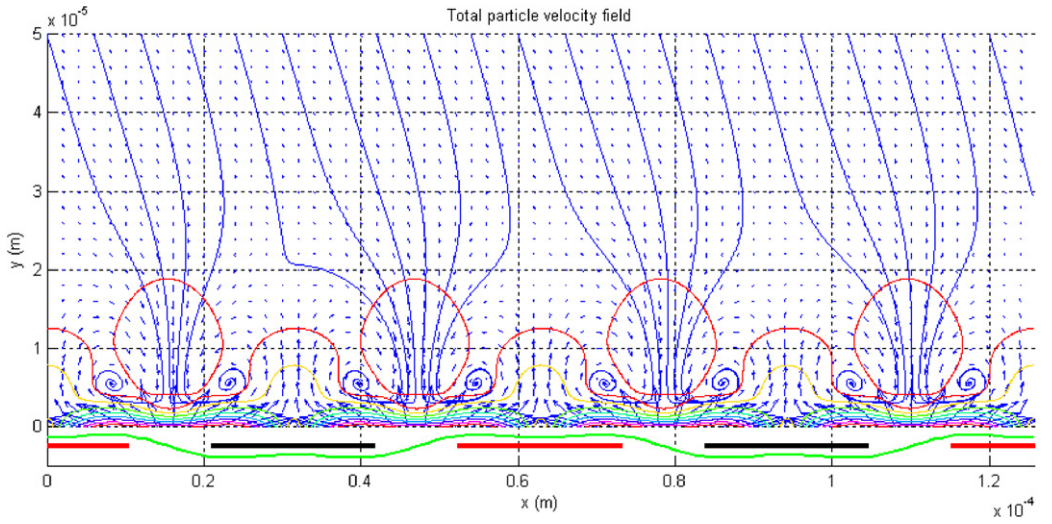

Fig. 13a. Total velocity diagram; concentration $= 0.13$, $dP/dx = 0.1$.

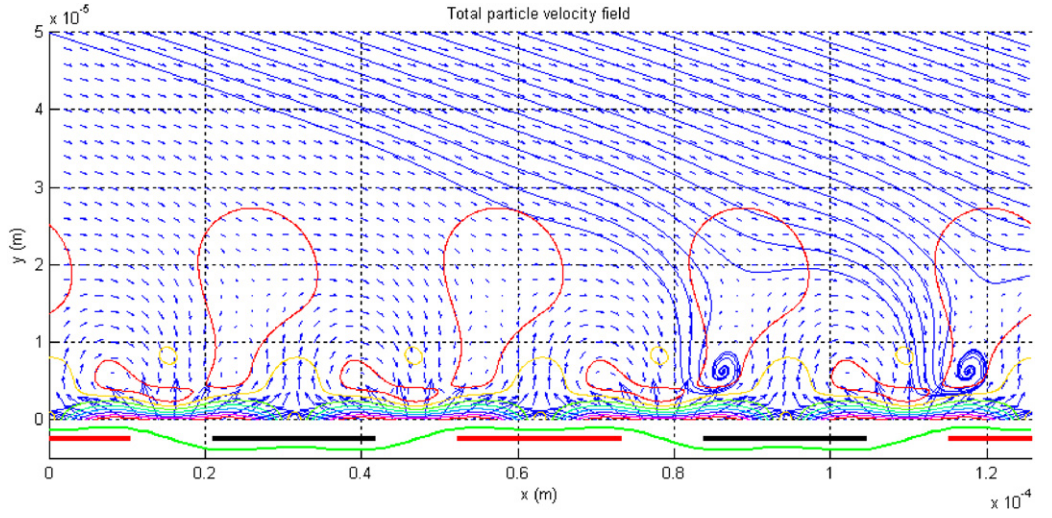

Fig. 13b. Total velocity field diagram; concentration $= 0.13$, $dP/dx = 1$.

Assuming Eq. (29) has no potential in conservative force field, i.e., $U(x) = 0$, and $\Phi = 1$ in Eq. (27). After simplification, Eqs. (29) and (30) is given as follows:

$$u_j = \frac{\phi_3 j(n-j)}{2\phi_2} + U_s$$

and

$$U_s = \frac{2}{3}\frac{\phi_3}{\phi_2}(\tau - 1)\tau.$$

Since $n \gg \tau$, U_s is omitted. And assuming $u_j \gg u_1(2qy - 1)\exp(-2qy)\sin(2qx)$, fluid velocity component ratio is represented as follows:

$$ratio = \frac{u_j}{u_1 2qy} = \frac{\frac{\phi_3 j(n-j)}{2\phi_2}}{\frac{p_0 y}{\eta}} = \frac{\frac{\frac{\delta_x F}{c\rho} j(n-j)}{2\phi_2}}{\frac{p_0 y}{\eta}} = \frac{\frac{(j\delta_x)(n-j)F}{2\phi_2 c\rho}}{\frac{p_0 y}{\eta}}. \tag{38}$$

For square lattice, $\delta_x = \delta_y$, $y = j\delta_y$,

$$ratio = \frac{(n-j)\eta F}{2\phi_2 p_0 c\rho} = \frac{F}{2\phi_2 p_0}\frac{(n-j)\delta_x(2\tau - 1)}{6} = \frac{F(2H - y)}{2p_0}$$

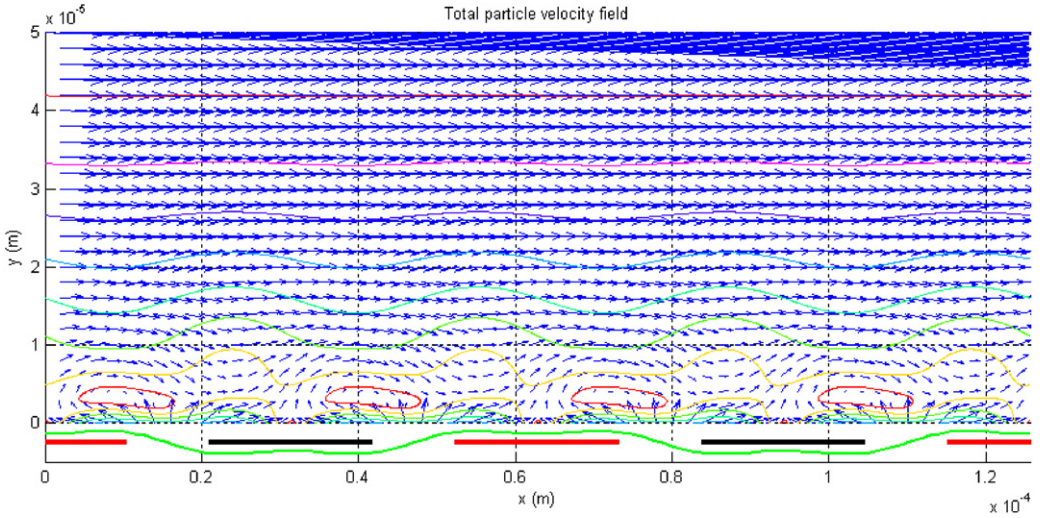

Fig. 13c. Total velocity field diagram; concentration $= 0.13$, $dP/dx = 10$.

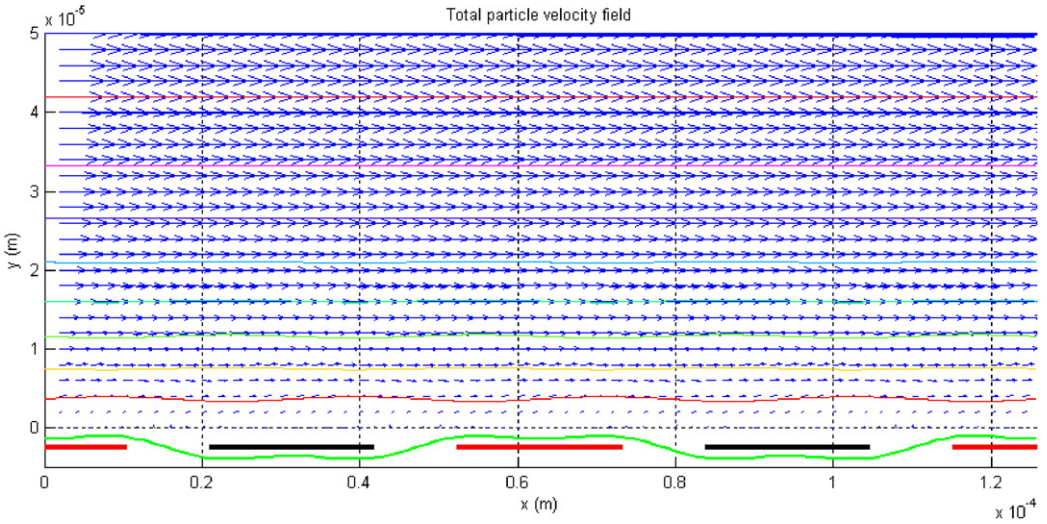

Fig. 13d. Total velocity field diagram; concentration $= 0.13$, $dP/dx = 100$.

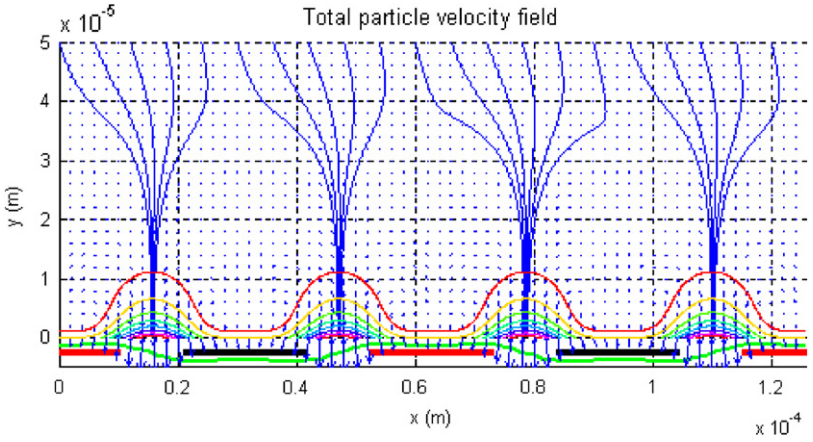

Fig. 14a. Total velocity field diagram; $dP/dx = 0.1$.

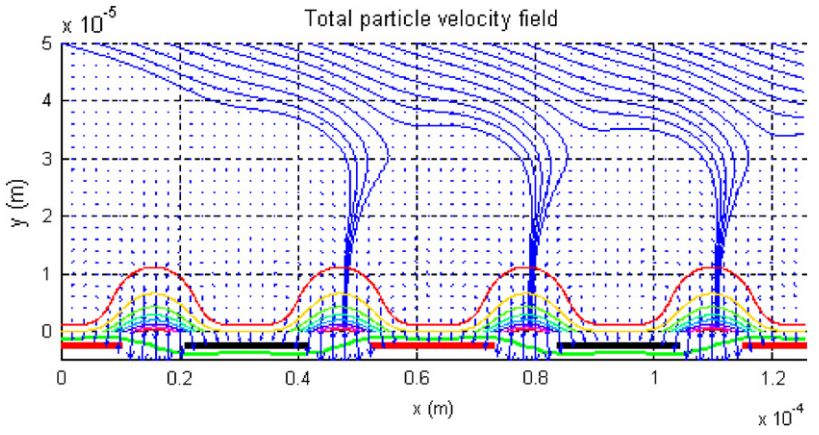

Fig. 14b. Total velocity field diagram; $dP/dx = 1$.

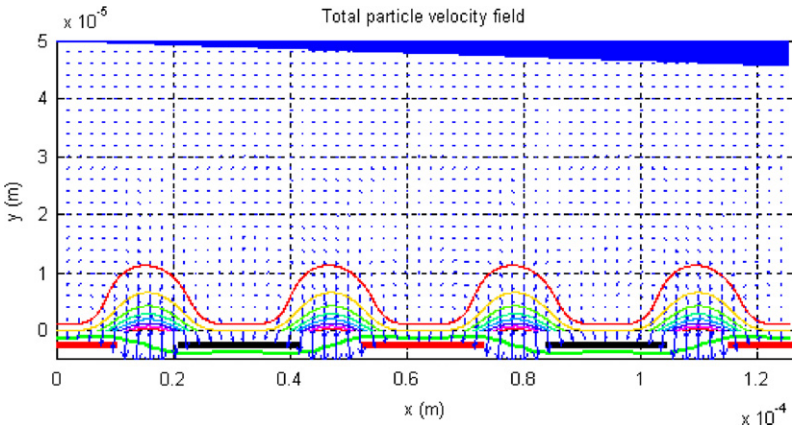

Fig. 14c. Total velocity field diagram; $dP/dx = 10$.

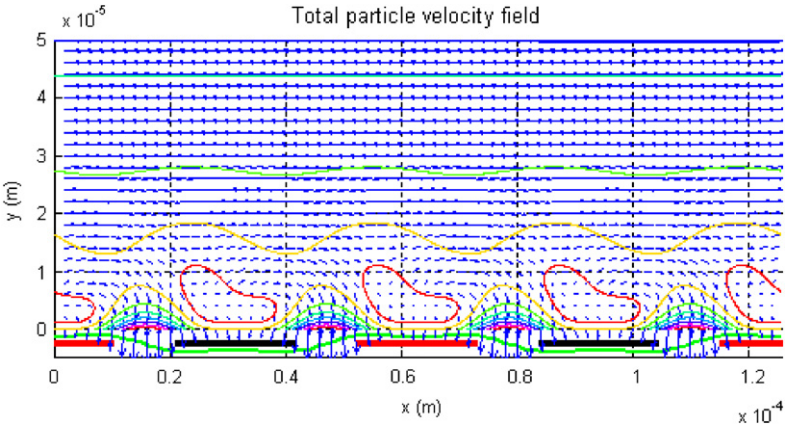

Fig. 14d. Total velocity field diagram; $dP/dx = 10^2$.

if$F$ excludes electric field effect and only dP/dx is considered, i.e.,

$$ratio = \frac{\frac{dP}{dx}}{\left(\frac{2p_0}{2H-y}\right)}. \tag{39}$$

$2H$ is flow channel height, $dP/dx = 1$, $p_0 = 8 \times 10^{-4}$, $2H = 1 \times 10^{-4}$, $y \ll 2H$ is used to substitute into Eq. (55) to obtain the ratio $= 1/16$. This substitution does not affect fluid flow. If $dP/dx = 10^2$, ratio $= 6$, fluid moves to x direction and carries away biological particles.

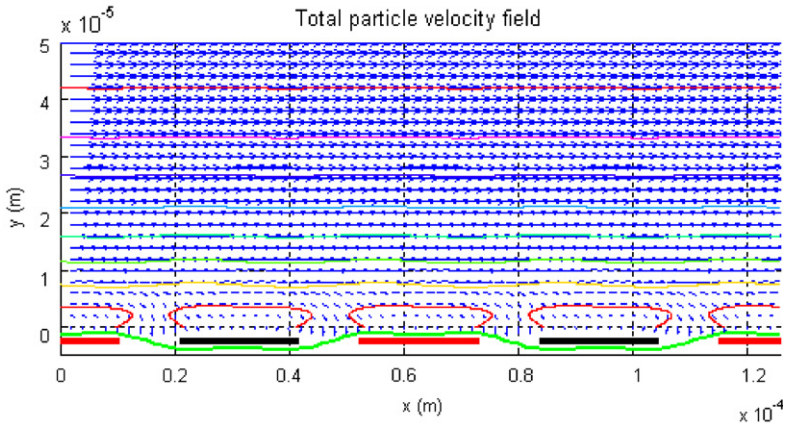

Fig. 14e. Total velocity field diagram; $dP/dx = 10^3$.

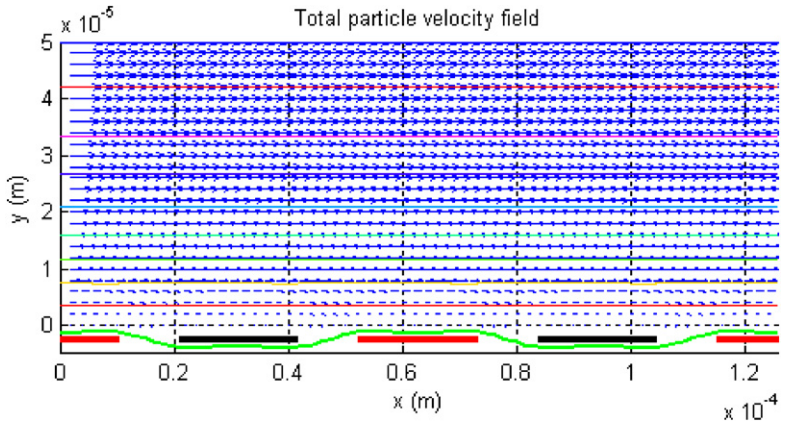

Fig. 14f. Total velocity field diagram; $dP/dx = 10^4$.

5. Conclusion

The present article uses LBM to simulate fluid behavior. Two main simulation models are presented. One is the cavity flow seeking solution where the traditional cavity flow problem is understood through observing the Reynolds number and relaxation coefficient. LBM is utilized to obtain velocity and flow line diagram, and Matlab is also utilized to develop software architecture for fluid dynamics computation to provide initial operation interface and function for fluid dynamics system program. The other model is applying an electrode voltage 0.25 V, AC electric field of frequency 98–846,801 Hz to a rectangular microchannel. Simulation is conducted on a fluid flow driven by different pressure gradients. The fluid velocity component ratio is also derived. The results indicate that the higher the ratio is, the more microparticles are flushed out. Selecting the proper ratio, it is able to absorb particles and carry away particles from electrode.

References

[1] B. Henrik, Theoretical Microfluidics, second ed., in: Lecture notes, 2005, pp. 101–139.
[2] M.S. Hung, O. Kurosawa, H. Kabata, M. Washizu, Stretching DNA fibers out of a chromosome in solution using electro-osmotic flow, 30 (4) 2009 pp. 289–295.
[3] M.F. Borges, S.L. Verardi, J.M. Machado, Electroosmotic pumping in rectangular microchannels: a numerical treatment by the finite element method, Appl. Math. E-Notes 2 (2002) 10–15.
[4] J. Donea, A. Huerta, Finite Element Methods for Flow Problem, John Wiley & Sons Ltd., 2003, 307–313.
[5] M.H. Oddy, J.G. Santiago, A method for determining electrophoretic and electroosmostic mobilities using AC and DC electric field particle displacements, J. Colloid Interface Sci. 269 (2004) 192–204.
[6] X. He, L.S. Luo, Theory of the lattice Boltzmann method: from the Boltzmann equation to the lattice Boltzmann equation, Phys. Rev. E 56 (6) (1997) 6811–6817.
[7] B. Li, D.Y. Kwok, A lattice Boltzmann model for electrokinetic microchannel flow of electrolyte solution in the presence of external forces with the Poisson–Boltzmann equation, Int. J. Heat Mass Transfer 46 (2003) 4235–4244.
[8] L.S. Thomas, S.P. Peder, E.V.P. Martin, Particle manipulation in microfluidics by AC electroosmosis and dielectrophoresis, Department of Micro and Nanotechnology Technical University of Denmark, 2006 pp. 1–57.
[9] X. He, Q. Zou, Analysis and boundary condition of the lattice Boltzmann BGK model with two velocity components, Cell. Autom. Lattice Gases (1995) 1–13.

[10] B. Li, D.Y. Kwok, Lattice Boltzmann model of microfluidics in the presence of external forces, J. Colloid Interface Sci. 263 (2003) 144–151.
[11] Q. Zou, X. He, On pressure and velocity flow boundary conditions for the lattice Boltzmann BGK model, Cell. Autom. Lattice Gases (1997) 1–20.
[12] Z. Guo, C. Zheng, B. Shi, An extrapolation method for boundary conditions in lattice Boltzmann method, Phys. Fluids 14 (6) (2002) 2007–2010.
[13] C.F. Hou, Development of boundary condition in lattice Boltzmann method, Master thesis, Department of Power Mechanical Engineering of National Tsing Hua University, Taiwan, 2006.
[14] J. Park, K.Y. Huh, X. Li, Lattice Boltzmann simulation on the junction potential in a microchannel, J. Electroanal. Chem. 591 (2006) 141–148.
[15] A. Ajdari, Pumping liquids using asymmetric electrode arrays, Phys. Rev. E 61 (1) (2000) 45–48.